

DETERMINATION OF GENERALIZED STRESS INTENSITY FACTORS FOR SHARP V-NOTCHED PLATES UNDER TRANSVERSE BENDING

Toshimi KONDO¹, Masato KUGAWA², Yohei KURABE³, Motojiro SUGISAWA⁴
Toru SASAKI¹, Masataka KOBAYASHI⁵

¹Department of Mechanical Engineering, Nagaoka National College of Technology

²Muratajyuki Corporations, 1-13-15 Sano Tochigi Prefecture

³Electrical & Mechanical Engineering Systems Engineering Advanced Course, Nagaoka National College of Technology

⁴Technical Section, General Affairs Division, Nagaoka National College of Technology

⁵Professor Emeritus, Nagaoka National College of Technology

The objective of this paper is to confirm the usefulness of the proposed method of determination for generalized stress intensity factors (GSIFs) of sharp V-notched plates under transverse bending based on Kirchhoff plate theory. First, by using the eigenfunction expansion method, singular strain fields in the neighborhood of the V-notch including the non-singular terms are derived. Second, using these strain fields, a theory of determining the GSIFs is presented under the condition of mixed mode loading. Finally, following the method, experiments on the specimens with various notch angles were performed for the mode I loading condition by using strain gages. The finite element analysis is also carried out to compare with the experimental results. The both results show good agreement between them.

Key Words: stress intensity factor, sharp V-notch, transverse bending, fracture mechanics, strain gage

1. INTRODUCTION

Sharp V-notches in structural components give rise localized stress concentration which decreases the maximum load-bearing capacity of the component, and may generate a crack or lead to early crack initiation. Notches may be regarded as sharp when the radius of curvature of their tips is very small compared with the length of the notch sides. Sharp angular corners of holes with machined notches can also be considered as sharp notches, and cracks can be regarded as particular sharp notches, for which the included angle is zero. If we take a polar coordinate system centered at the tip of a notch angle 2β , the stresses near the notch tip can be expressed as $\sigma \cong K_{I,\lambda} r^{\lambda-1} f_1(\theta) + K_{II,\gamma} r^{\gamma-1} f_2(\theta)$, where λ and γ are the characteristic values depending on the notch angle between two stress-free boundaries, and $K_{I,\lambda}$ and $K_{II,\gamma}$ are called as the generalized

stress intensity factors of mode I and mode II, respectively. Thus, for given geometry of components and loading conditions, $K_{I,\lambda}$ and $K_{II,\gamma}$ completely characterize the stress state in the region near the notch tip, and are a key factor in solving the problems related to the strength evaluation of materials¹⁾, crack initiation^{2),3)} and the application to the fatigue⁴⁾ of notched materials under the cyclic loading. The limiting case of the notch angle $2\beta=0$ corresponds to a crack, and $\lambda-1=\gamma-1=-1/2$, $\theta=0$ and $\sigma=K_I r^{-1/2} + K_{II} r^{-1/2}$, where K_I and K_{II} are widely-used stress intensity factors of linear fracture mechanics. Since the pioneer works of Williams⁵⁾, over the past decades, a number of studies have been conducted on the singular stress fields of the V-notched plates by the various methods of solution, such as collocation methods^{6),7)}, finite element methods^{8),9)}, boundary element methods¹⁰⁾, and theoretical analyses^{11),12)}. However, only a few works concerned with those problems

have been studied on experimental procedures, such as the method of caustics^{13), 14)}, the photoelastic technology¹⁵⁾ and recently the coherent gradient method¹⁶⁾. In the previous papers, the strain gage method of determination of GSIFs at the sharp V-notched plate have been developed, where the V-notched plate under tension¹⁷⁾ and in plane bending¹⁸⁾ were treated.

In this paper, the strain gage method is applied to the determination of GSIFs at the V-notch of the plate under transverse bending. The Kirchhoff¹⁹⁾ plate theory is used. The eigenfunction expansions together with complex functions are employed to derive the singular strain fields in the neighborhood at the tip of the V-notch including the non-singular terms. Second, using these strain fields, a theory of determining the GSIFs is presented under the condition of mixed mode loading. Finally, following the method, experiments on the specimens with three types of notch angle using strain gages were performed for the mode I loading condition. The finite element analysis is also carried out to compare with the experimental results. The both results show good agreement between them and as a result they are influenced on the notch angle.

2. SINGULAR STRAIN FIELDS AROUND THE V-NOTCH

The plate with a sharp V-notch is subjected to a transverse bending load as shown in **Fig.1**. Let (r, θ) be a polar coordinate system centered at the tip of the V-notch, such that the line $\theta=0$ axis is bisector of the notch angle 2β , and the angle between the x-axis and the line perpendicular to the straight side of the plate is denoted by ω . The length of line from the notch tip to the side of the plate, which is perpendicular to the plate side as shown in Fig.1, is denoted by a .

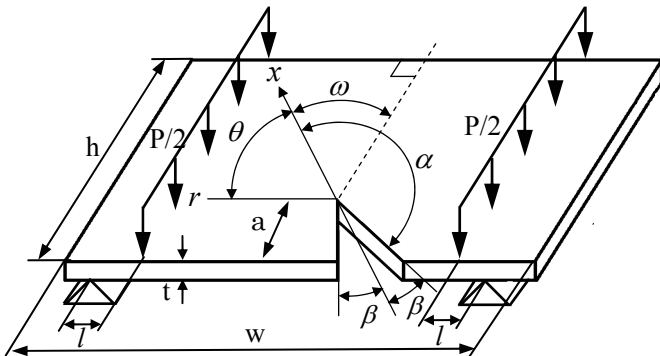


Fig.1 Transverse bending of V-notched plates and the coordinate systems

On the basis of Kirchhoff plate theory¹⁹⁾, the strain components ε_{rr} , $\varepsilon_{\theta\theta}$, $\varepsilon_{r\theta}$ of the plate free from lateral loads is expressed in terms of two complex potential functions $\varphi(z)$ and $\psi(z)$ ²⁰⁾:

$$\varepsilon_{rr} + \varepsilon_{\theta\theta} = -2\delta \left[\varphi'(z) + \overline{\varphi'(z)} \right] \quad (1)$$

$$\varepsilon_{\theta\theta} - \varepsilon_{rr} + i\varepsilon_{r\theta} = 2\delta \left[z\varphi''(z) + \psi'(z) \right] e^{2i\theta} \quad (2)$$

where $z = re^{i\theta}$, and δ denotes a distance from the mid-plane in an un-deformed plate to any point including the surface of the plate. From the stress-strain relations, the stress components σ_{rr} , $\sigma_{\theta\theta}$, $\sigma_{r\theta}$ corresponding to eqs. (1) and (2) are derived:

$$\sigma_{rr} + \sigma_{\theta\theta} = -\frac{2E\delta}{1-\nu} \left[\varphi'(z) + \overline{\varphi'(z)} \right] \quad (3)$$

$$\sigma_{\theta\theta} - \sigma_{rr} + 2i\sigma_{r\theta} = \frac{2\delta}{1+\nu} \left[z\varphi''(z) + \psi'(z) \right] e^{2i\theta} \quad (4)$$

where ν is Poisson's ratio, and E is Young's modulus of the plate. To obtain singular strain fields to the present problem, the eigenfunction expansion method is used.

We assume the complex potential functions of $\varphi(z)$ and $\psi(z)$ near the tip of the V-notched plate analogous to the plane problems¹⁷⁾, as follows:

$$\varphi(z) = \sum_{n=1}^{\infty} (A_n z^{\lambda_n} + iB_n z^{\gamma_n}) \quad (5)$$

$$\psi(z) = \sum_{n=1}^{\infty} \left[-A_n \{ \kappa \cos 2(\lambda_n - 1)\alpha + 1 + (\lambda_n - 1)\cos 2\alpha \} z^{\lambda_n} \right. \\ \left. + iB_n \{ \kappa \cos 2(\gamma_n - 1)\alpha - 1 - (\gamma_n - 1)\cos 2\alpha \} z^{\gamma_n} \right] \quad (6)$$

where A_n and B_n are real numbers determined by the boundary conditions, and $\kappa = -(3 + \nu)/(1 - \nu)$. The eigenvalue of λ_n and γ_n correspond to mode I and mode II, respectively, which satisfy the following characteristic equations:

$$\sin 2\alpha(\lambda_n - 1) + \kappa\lambda_n \sin 2\alpha = 0 \quad (7)$$

$$\sin 2\alpha(\gamma_n - 1) - \kappa(\gamma_n - 1)\sin 2\alpha = 0 \quad (8)$$

which are derived from the stress free boundary condition along the two notch sides. It is noted that the eigenvalues are influenced by the notch angles as well as Poisson's ratio ν . Substituting eqs.(5) and (6) into eqs.(1) and (2), we obtain

$$\varepsilon_{rr} = \delta \sum_{n=1}^{\infty} \left\langle A_n \lambda_n r^{\lambda_n - 1} \left[(-1 - \lambda_n)\cos(\lambda_n - 1)\theta + \right. \right. \\ \left. \left. + \{ \kappa \cos 2\alpha(\lambda_n - 1) + (\lambda_n - 1)\cos 2\alpha + 1 \} \cos(\lambda_n + 1)\theta \right] \right. \\ \left. + \delta \sum_{n=1}^{\infty} \left\langle B_n \gamma_n r^{\gamma_n - 1} \left[(1 + \gamma_n)\cos(\gamma_n - 1)\theta + \right. \right. \\ \left. \left. + \{ \kappa \cos 2\alpha(\gamma_n - 1) - (\gamma_n - 1)\cos 2\alpha - 1 \} \sin(\gamma_n + 1)\theta \right] \right\rangle \quad (9)$$

$$\begin{aligned}
 \varepsilon_{\theta\theta} &= \delta \sum_{n=1}^{\infty} \left\langle A_n \lambda_n r^{\lambda_n - 1} [(-3 - \lambda_n) \cos(\lambda_n - 1)\theta - \right. \\
 &\quad \left. - \{\kappa \cos 2\alpha(\lambda_n - 1) + (\lambda_n - 1) \cos 2\alpha + 1\} \cos(\lambda_n + 1)\theta \right\rangle + \\
 &\quad + \delta \sum_{n=1}^{\infty} \left\langle B_n \gamma_n r^{\gamma_n - 1} [(3 - \gamma_n) \sin(\gamma_n - 1)\theta - \right. \\
 &\quad \left. - \{\kappa \cos 2\alpha(\gamma_n - 1) - (\gamma_n - 1) \cos 2\alpha - 1\} \sin(\gamma_n + 1)\theta \right\rangle \quad (10) \\
 \varepsilon_{r\theta} &= 2\delta \sum_{n=1}^{\infty} \left\langle A_n \lambda_n r^{\lambda_n - 1} [(-1 + \lambda_n) \sin(\lambda_n - 1)\theta - \right. \\
 &\quad \left. - \{\kappa \cos 2\alpha(\lambda_n - 1) + (\lambda_n - 1) \cos 2\alpha + 1\} \sin(\lambda_n + 1)\theta \right\rangle + \\
 &\quad + 2\delta \sum_{n=1}^{\infty} \left\langle B_n \gamma_n r^{\gamma_n - 1} [(-1 + \gamma_n) \cos(\gamma_n - 1)\theta + \right. \\
 &\quad \left. + \{\kappa \cos 2\alpha(\gamma_n - 1) - (\gamma_n - 1) \cos 2\alpha - 1\} \cos(\gamma_n + 1)\theta \right\rangle \quad (11)
 \end{aligned}$$

The first non-zero eigenvalues of λ_1 and γ_1 of the above eqs.(7) and (8) are real, where $1/2 < \lambda_1 \leq 1$ and $1/2 < \gamma_1 \leq 1$ for $\pi/2 < \alpha \leq \pi$, and therefore the strains in eqs.(9),(10) and (11) have singularity at the notch tip and expressed by

$$\begin{aligned}
 \varepsilon_{rr} &= \delta \left\langle A_1 \lambda_1 r^{\lambda_1 - 1} [(-1 - \lambda_1) \cos(\lambda_1 - 1)\theta + \right. \\
 &\quad \left. + \{\kappa \cos 2\alpha(\lambda_1 - 1) + (\lambda_1 - 1) \cos 2\alpha + 1\} \cos(\lambda_1 + 1)\theta \right\rangle + \\
 &\quad + \delta \left\langle B_1 \gamma_1 r^{\gamma_1 - 1} [(1 + \gamma_1) \cos(\gamma_1 - 1)\theta + \right. \\
 &\quad \left. + \{\kappa \cos 2\alpha(\gamma_1 - 1) - (\gamma_1 - 1) \cos 2\alpha - 1\} \sin(\gamma_1 + 1)\theta \right\rangle \quad (12)
 \end{aligned}$$

$$\begin{aligned}
 \varepsilon_{\theta\theta} &= \delta \left\langle A_1 \lambda_1 r^{\lambda_1 - 1} [(-3 + \lambda_1) \cos(\lambda_1 - 1)\theta - \right. \\
 &\quad \left. - \{\kappa \cos 2\alpha(\lambda_1 - 1) + (\lambda_1 - 1) \cos 2\alpha + 1\} \cos(\lambda_1 + 1)\theta \right\rangle + \\
 &\quad + \delta \left\langle B_1 \gamma_1 r^{\gamma_1 - 1} [(3 - \gamma_1) \sin(\gamma_1 - 1)\theta - \right. \\
 &\quad \left. - \{\kappa \cos 2\alpha(\gamma_1 - 1) - (\gamma_1 - 1) \cos 2\alpha - 1\} \sin(\gamma_1 + 1)\theta \right\rangle \quad (13)
 \end{aligned}$$

$$\begin{aligned}
 \varepsilon_{r\theta} &= 2\delta \left\langle A_1 \lambda_1 r^{\lambda_1 - 1} [(-1 + \lambda_1) \sin(\lambda_1 - 1)\theta - \right. \\
 &\quad \left. - \{\kappa \cos 2\alpha(\lambda_1 - 1) + (\lambda_1 - 1) \cos 2\alpha + 1\} \sin(\lambda_1 + 1)\theta \right\rangle + \\
 &\quad + 2\delta \left\langle B_1 \gamma_1 r^{\gamma_1 - 1} [(-1 + \gamma_1) \cos(\gamma_1 - 1)\theta + \right. \\
 &\quad \left. + \{\kappa \cos 2\alpha(\gamma_1 - 1) - (\gamma_1 - 1) \cos 2\alpha - 1\} \cos(\gamma_1 + 1)\theta \right\rangle \quad (14)
 \end{aligned}$$

Similarly, the singular stress components σ_{rr} , $\sigma_{\theta\theta}$, $\sigma_{r\theta}$ are derived by eqs.(3) and (4) for $n=1$, as follows:

$$\begin{aligned}
 \sigma_{rr} &= E\delta/(1 - \nu^2) \left\langle A_1 \lambda_1 r^{\lambda_1 - 1} [(-1 - \lambda_1) \cos(\lambda_1 - 1)\theta + \right. \\
 &\quad \left. + \{\kappa \cos 2\alpha(\lambda_1 - 1) + (\lambda_1 - 1) \cos 2\alpha + 1\} \cos(\lambda_1 + 1)\theta \right\rangle + \\
 &\quad + E\delta/(1 - \nu^2) \left\langle B_1 \gamma_1 r^{\gamma_1 - 1} [(1 + \gamma_1) \cos(\gamma_1 - 1)\theta + \right. \\
 &\quad \left. + \{\kappa \cos 2\alpha(\gamma_1 - 1) - (\gamma_1 - 1) \cos 2\alpha - 1\} \sin(\gamma_1 + 1)\theta \right\rangle \quad (15)
 \end{aligned}$$

$$\begin{aligned}
 \sigma_{\theta\theta} &= E\delta/(1 - \nu^2) \left\langle A_1 \lambda_1 r^{\lambda_1 - 1} [(-3 + \lambda_1) \cos(\lambda_1 - 1)\theta - \right. \\
 &\quad \left. - \{\kappa \cos 2\alpha(\lambda_1 - 1) + (\lambda_1 - 1) \cos 2\alpha + 1\} \cos(\lambda_1 + 1)\theta \right\rangle + \\
 &\quad + E\delta/(1 - \nu^2) \left\langle B_1 \gamma_1 r^{\gamma_1 - 1} [(3 - \gamma_1) \sin(\gamma_1 - 1)\theta - \right. \\
 &\quad \left. - \{\kappa \cos 2\alpha(\gamma_1 - 1) - (\gamma_1 - 1) \cos 2\alpha - 1\} \sin(\gamma_1 + 1)\theta \right\rangle \quad (16)
 \end{aligned}$$

$$\begin{aligned}
 \sigma_{r\theta} &= E\delta/(1 + \nu) \left\langle A_1 \lambda_1 r^{\lambda_1 - 1} [(-1 + \lambda_1) \sin(\lambda_1 - 1)\theta - \right. \\
 &\quad \left. - \{\kappa \cos 2\alpha(\lambda_1 - 1) + (\lambda_1 - 1) \cos 2\alpha + 1\} \sin(\lambda_1 + 1)\theta \right\rangle + \\
 &\quad + E\delta/(1 + \nu) \left\langle B_1 \gamma_1 r^{\gamma_1 - 1} [(-1 + \gamma_1) \cos(\gamma_1 - 1)\theta + \right. \\
 &\quad \left. + \{\kappa \cos 2\alpha(\gamma_1 - 1) - (\gamma_1 - 1) \cos 2\alpha - 1\} \cos(\gamma_1 + 1)\theta \right\rangle \quad (17)
 \end{aligned}$$

In this study, the GSIFs of $K_{I,\lambda}$ and $K_{II,\gamma}$ are defined, following by Chen¹¹, as follows:

$$K_{I,\lambda_1} = \lim_{r \rightarrow 0, \theta = 0} \sqrt{2\pi r}^{1-\lambda_1} \sigma_{\theta\theta}(r, \theta) \quad (18)$$

$$K_{II,\gamma_1} = (3 + \nu)/(1 + \nu) \lim_{r \rightarrow 0, \theta = 0} \sqrt{2\pi r}^{1-\gamma_1} \sigma_{r\theta}(r, \theta) \quad (19)$$

The coefficient $(3 + \nu)/(1 + \nu)$ in the right hand side of eq.(19) is added to satisfy the consistency to the plane problems. Substituting eqs.(16) and (17) into eqs.(18) and (19), we obtain

$$A_1 = \frac{K_{I,\lambda_1}}{\sqrt{2\pi}} \frac{1 - \nu^2}{E\delta} \frac{1}{\lambda C_{II}}, \quad B_1 = \frac{K_{II,\gamma_1}}{\sqrt{2\pi}} \frac{1 + \nu}{E\delta} \frac{1}{\gamma_1 C_{II}} \quad (20),(21)$$

$$C_I = \{-3 - \nu + \lambda_1(1 - \nu)\} - (1 - \nu) \{\kappa \cos 2\alpha(\lambda_1 - 1) + (\lambda_1 - 1) \cos 2\alpha\} \quad (22)$$

$$C_{II} = \gamma_1 - 1 + \{\kappa \cos 2\alpha(\gamma_1 - 1) - 1 - (\gamma_1 - 1) \cos 2\alpha\} \quad (23)$$

Thus we obtain the singular strain fields near the V-notch in the final form including the non-singular terms f_{r3} , $f_{\theta3}$, $f_{r\theta}$ as follows:

$$\begin{aligned}
 \varepsilon_{rr} &= -\frac{K_{I,\lambda_1} (1 - \nu^2)}{\sqrt{2\pi} E r^{1-\lambda_1}} \frac{[C_I \cos(\lambda_1 + 1)\theta + (\lambda_1 + 1) \cos(\lambda_1 - 1)\theta]}{[C_I(1 - \nu) - 3 - \nu + \lambda_1(1 - \nu)]} + \\
 &\quad + \frac{K_{II,\gamma_1} (1 + \nu)^2}{\sqrt{2\pi} E r^{1-\gamma_1}} \frac{[C_{II} \sin(\gamma_1 + 1)\theta + (\gamma_1 + 1) \sin(\gamma_1 - 1)\theta]}{(3 + \nu) [C_{II} + (\gamma_1 - 1)]} + f_{r3} \\
 \varepsilon_{\theta\theta} &= \frac{K_{I,\lambda_1} (1 - \nu^2)}{\sqrt{2\pi} E r^{1-\lambda_1}} \frac{[C_I \cos(\lambda_1 + 1)\theta + (\lambda_1 - 3) \cos(\lambda_1 - 1)\theta]}{[C_I(1 - \nu) - 3 - \nu + \lambda_1(1 - \nu)]} - \\
 &\quad - \frac{K_{II,\gamma_1} (1 + \nu)^2}{\sqrt{2\pi} E r^{1-\gamma_1}} \frac{[C_{II} \sin(\gamma_1 + 1)\theta + (\gamma_1 - 3) \sin(\gamma_1 - 1)\theta]}{(3 + \nu) [C_{II} + (\gamma_1 - 1)]} + f_{\theta3} \\
 \varepsilon_{r\theta} &= \frac{K_{I,\lambda_1} \cdot 2(1 - \nu^2)}{\sqrt{2\pi} E r^{1-\lambda_1}} \frac{[C_I \sin(\lambda_1 + 1)\theta + (\lambda_1 - 1) \sin(\lambda_1 - 1)\theta]}{[C_I(1 - \nu) - 3 - \nu + \lambda_1(1 - \nu)]} + \\
 &\quad + \frac{K_{II,\gamma_1} \cdot 2(1 + \nu)^2}{\sqrt{2\pi} E r^{1-\gamma_1}} \frac{[C_{II} \cos(\gamma_1 + 1)\theta + (\gamma_1 - 1) \cos(\gamma_1 - 1)\theta]}{(3 + \nu) [C_{II} + \gamma_1 - 1]} + f_{r\theta} \quad (24),(25),(26)
 \end{aligned}$$

Similarly, for the singular stress fields:

$$\begin{aligned}
 \sigma_{rr} &= -\frac{K_{I,\lambda_1}}{\sqrt{2\pi} r^{1-\lambda_1}} \times \\
 &\quad \times \frac{[C_I(1 - \nu) \cos(\lambda_1 + 1)\theta + \{1 + 3\nu + \lambda_1(1 - \nu)\} \cos(\lambda_1 - 1)\theta]}{[C_I(1 - \nu) - 3 - \nu + \lambda_1(1 - \nu)]} + \\
 &\quad + \frac{K_{II,\gamma_1}}{\sqrt{2\pi} r^{1-\gamma_1}} \cdot \frac{(1 + \nu)}{(3 + \nu)(1 - \nu)} \times \\
 &\quad \times \frac{[C_{II}(1 - \nu) \sin(\gamma_1 + 1)\theta + \{1 + 3\nu + \gamma_1(1 - \nu)\} \sin(\gamma_1 - 1)\theta]}{[C_{II} + (\gamma_1 - 1)]} + f_{rr}^*
 \end{aligned}$$

$$\begin{aligned}
 \sigma_{\theta\theta} &= \frac{K_{I,\lambda_1}}{\sqrt{2\pi r}^{1-\lambda_1}} \times \\
 &\times \frac{[C_I(1-\nu)\cos(\lambda_1+1)\theta - \{3+\nu-\lambda_1(1-\nu)\}\cos(\lambda_1-1)\theta]}{[C_I(1-\nu)-3-\nu+\lambda_1(1-\nu)]} - \\
 &- \frac{K_{II,\gamma_1}}{\sqrt{2\pi r}^{1-\gamma_1}} \cdot \frac{(1+\nu)}{(1-\nu)(3+\nu)} \times \\
 &\times \frac{[C_{II}(1-\nu)\sin(\gamma_1+1)\theta - \{3+\nu-\gamma_1(1-\nu)\}\sin(\gamma_1-1)\theta]}{[C_{II}+(\gamma_1-1)]} + f_{r\theta}^* \\
 \sigma_{r\theta} &= \frac{K_{I,\lambda_1}}{\sqrt{2\pi r}^{1-\lambda_1}} \cdot (1-\nu) \times \\
 &\times \frac{[C_I \sin(\lambda_1+1)\theta + (\lambda_1-1)\sin(\lambda_1-1)\theta]}{[C_I(1-\nu)-3-\nu+\lambda_1(1-\nu)]} + \\
 &+ \frac{K_{II,\gamma_1}}{\sqrt{2\pi r}^{1-\gamma_1}} \cdot \frac{(1+\nu)}{(3+\nu)} \times \frac{[C_{II} \cos(\gamma_1+1)\theta + (\gamma_1-1)\cos(\gamma_1-1)\theta]}{[C_{II}+\gamma_1-1]} + \\
 &+ f_{r\theta}^*
 \end{aligned} \tag{27),(28),(29)$$

where f_{r3}^* , $f_{\theta\theta 3}^*$, $f_{r\theta 3}^*$ is also non-singular terms. If we put $\alpha = \pi$, $\lambda_1 = \gamma_1 = 1/2$, i.e., for the special case of a crack, the singular strain and stress fields are obtained from eqs.(24)~(29), as follows:

$$\begin{aligned}
 \varepsilon_{rr} &\cong -\frac{K_I}{\sqrt{2\pi r}} \frac{(1+\nu)}{4E(3+\nu)} \left[(7+\nu)\cos\frac{3\theta}{2} + 3(\nu-1)\cos\frac{\theta}{2} \right] + \\
 &+ \frac{K_{II}}{\sqrt{2\pi r}} \frac{(1+\nu)}{4E(3+\nu)} \left[(5+3\nu)\sin\frac{3\theta}{2} + 3(\nu-1)\sin\frac{\theta}{2} \right] + f_{r3} \\
 \varepsilon_{\theta\theta} &\cong \frac{K_I}{\sqrt{2\pi r}} \frac{(1+\nu)}{4E(3+\nu)} \left[(7+\nu)\cos\frac{3\theta}{2} + 5(1-\nu)\cos\frac{\theta}{2} \right] \\
 &- \frac{K_{II}}{\sqrt{2\pi r}} \frac{(1+\nu)}{4E(3+\nu)} \left[(5+3\nu)\sin\frac{3\theta}{2} + 5(1-\nu)\sin\frac{\theta}{2} \right] + f_{\theta 3} \\
 \varepsilon_{r\theta} &\cong \frac{K_I}{\sqrt{2\pi r}} \frac{(7+\nu)}{4G(3+\nu)} \left[\sin\frac{3\theta}{2} - \frac{(1-\nu)}{(7+\nu)}\sin\frac{\theta}{2} \right] + \\
 &+ \frac{K_{II}}{\sqrt{2\pi r}} \frac{(5+3\nu)}{4G(3+\nu)} \left[\cos\frac{3\theta}{2} - \frac{(1-\nu)}{(5+3\nu)}\cos\frac{\theta}{2} \right] + f_{r\theta 3}
 \end{aligned} \tag{30),(31),(32)$$

$$\begin{aligned}
 \sigma_{rr} &\cong -\frac{K_I}{\sqrt{2\pi r}} \frac{(7+\nu)}{4(3+\nu)} \left[\cos\frac{3\theta}{2} - \frac{3+5\nu}{7+\nu}\cos\frac{\theta}{2} \right] + \\
 &+ \frac{K_{II}}{\sqrt{2\pi r}} \frac{(5+3\nu)}{4(3+\nu)} \left[\sin\frac{3\theta}{2} - \frac{3+5\nu}{5+3\nu}\sin\frac{\theta}{2} \right] + f_{r3}^* \\
 \sigma_{\theta\theta} &\cong \frac{K_I}{\sqrt{2\pi r}} \frac{(7+\nu)}{4(3+\nu)} \left[\cos\frac{3\theta}{2} + \frac{5+3\nu}{7+\nu}\cos\frac{\theta}{2} \right] - \\
 &- \frac{K_{II}}{\sqrt{2\pi r}} \frac{(5+3\nu)}{4(3+\nu)} \left[\sin\frac{3\theta}{2} + \sin\frac{\theta}{2} \right] + f_{\theta 3}^*
 \end{aligned}$$

$$\begin{aligned}
 \sigma_{r\theta} &\cong \frac{K_I}{\sqrt{2\pi r}} \frac{(7+\nu)}{4(3+\nu)} \left[\sin\frac{3\theta}{2} - \frac{(1-\nu)}{(7+\nu)}\sin\frac{\theta}{2} \right] + \\
 &+ \frac{K_{II}}{\sqrt{2\pi r}} \frac{(5+3\nu)}{4(3+\nu)} \left[\cos\frac{3\theta}{2} - \frac{(1-\nu)}{(5+3\nu)}\cos\frac{\theta}{2} \right] + f_{r\theta 3}^*
 \end{aligned} \tag{33),(34),(35)$$

These equations are coinciding with those obtained by Williams²¹⁾ for the crack problem under transverse bending.

3. PROCEDURE OF DETERMINATION OF GSIFs

In the mixed loading condition, to separate the GSIFs $K_{I,\lambda}$ and $K_{I,\gamma}$, we must measure the strains along more than two points in any directions and the line extending from the notch tip. Basically, although both strains ε_{rr} and $\varepsilon_{\theta\theta}$ can be available to obtain $K_{I,\lambda}$ and $K_{I,\gamma}$, we used ε_{rr} in this study. The strip strain gages consisting of five measuring grids are positioned along the two directions of $\theta = \theta_1$ and θ_2 measured from the extension of the bisector of the notch angle as shown in **Fig.2**. We denote the strains of the five points in the directions θ_1 and θ_2 as ε_{r1i} and ε_{r2i} ($i = 1, \dots, 5$), respectively. Moreover, the distances from the notch tip to each center of strain gage position in the direction of θ_1 and θ_2 are denoted by r_{1i} and r_{2i} , respectively (see Fig.2). Substituting the measured quantities of ε_{r1i} and r_{1i} into eq.(24), we obtain the basic expressions to separate GSIFs of $K_{I,\lambda}$ and $K_{I,\gamma}$ under mixed mode conditions as follows:

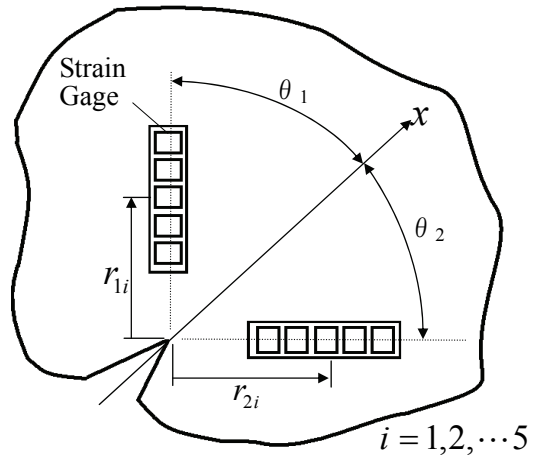


Fig.2 Strain gage positions and directions

$$Z_1(\varepsilon_{r_{ji}}, r_{ji}) = A_1 X_1(r_{ji}) + B_1 Y_1(r_{ji}) + K_{I,\lambda_1} \quad (36)$$

$$Z_2(\varepsilon_{r_{ji}}, r_{ji}) = A_2 X_2(r_{ji}) + B_2 Y_2(r_{ji}) + K_{II,\gamma_1} \quad (37)$$

$(i = 1, 2, \dots, 5 ; j = 1, 2)$

where X_j and Y_j are the functions of only r_{ji} , and A_j and B_j are constants that do not include $\varepsilon_{r_{1i}}$ and $\varepsilon_{r_{2i}}$ (see Appendix). Equations (36) and (37) express the plane in the three dimensional coordinates (X_j, Y_j, Z_j) and show that $K_{I,\lambda}$ and $K_{II,\gamma}$ can be obtained from the intersection of the Z_j -axis (see **Fig.3**) and the plane constructed by the least squares method using the strains $\varepsilon_{r_{1i}}$ measured in the two directions θ_1 and θ_2 as shown in **Fig.2**.

4. EXPERIMENTAL PROCEDURE AND FINITE ELEMENT ANALYSIS

4.1 Test Specimen and Experiment

Experiments are performed to demonstrate the method described above. Transverse bending specimens with $w=500\text{mm}$ width and $h=100\text{mm}$ length made of aluminum 5052 alloy, which fabricated from a 8mm thick plate, were used (see **Fig.1**). Three types of notch angles corresponding to the mode I loading condition were machined by the wire electric discharge machine with a wire of 0.03mm diameter (see **Table 1**). Thus, the radius of curvature of the notch tip is 0.015 mm and is very small compared with the notch sides, and it may be regarded as the sharp notch. Mechanical properties of the specimens are summarized in **Table 2**. Strain gages with five element grids with gage length is 1mm (Kyowa Company, KFG-1-120-Da-23N-10C2) were positioned along the line

$\theta_1 = -\theta_2 = 90\text{deg}$ to obtain still larger strains. The CCD camera with 0.01mm accuracy was used to measuring the distances from the each strain gage position r_{ji} ($j = 1, 2 ; i = 1, \dots, 5$) (see **Table 3**). The suitable location of strain gage was referred to the results studied by Dally and Sanford²²⁾ for the crack problem. The transverse bending moment was carried out by the four-point bending apparatus from 100N to 220N by the digital-testing machine. The magnitude of the loads are determined to hold the small scale yielding condition in linear fracture mechanics, specifically we took the radius of plastic zone size as within 0.1mm. Here, the following non-dimensional notations are used:

$$K_{I,\lambda_1}^* = \frac{K_{I,\lambda_1}}{\sigma_0 \sqrt{\pi a}^{1-\lambda_1}}, \quad K_{II,\gamma_1}^* = \frac{K_{II,\gamma_1}}{\sigma_0 \sqrt{\pi a}^{1-\gamma_1}} \quad (38),(39)$$

where $\sigma_0 = 3P\ell / wt^2$ and ℓ is the distance from the support to the loading position of the plate (see **Fig.1**). It should be noted that the theoretical values K_{I,λ_1}^* and K_{II,γ_1}^* may be independent of the load for the given notch angles and shapes.

4.2 Finite Element Analysis

Finite element analysis (FEA) based on the Kirchhoff plate theory was performed to compare with the results of the experiments. Configurations and boundary conditions of the specimens used in the analysis are the same as those in the experiments. In the finite element analysis, we used the [ANSYS] for each specimen, following by the method outlined in the previous chapter. **Figure 4** shows the typical finite element mesh for the analysis, consisting 8680 elements and 8109 nodes, and the most fine mesh length is 10^{-7} m near the

Table 1 Specimen dimensions

Specimen	2β (deg)	λ_1	γ_1	ω (deg)	h (mm)	w (mm)	a (mm)	t (mm)
A	0	0.5	0.5					
B	30	0.55498	0.53625	0	100	500	25	8
C	60	0.62031	0.58097					

Table 2 Mechanical properties of the specimen

Young's Modulus (GPa)	Poisson's Ratio	Yield Strength (MPa)	Tensile Strength (MPa)
70.3	0.34	91.1	197

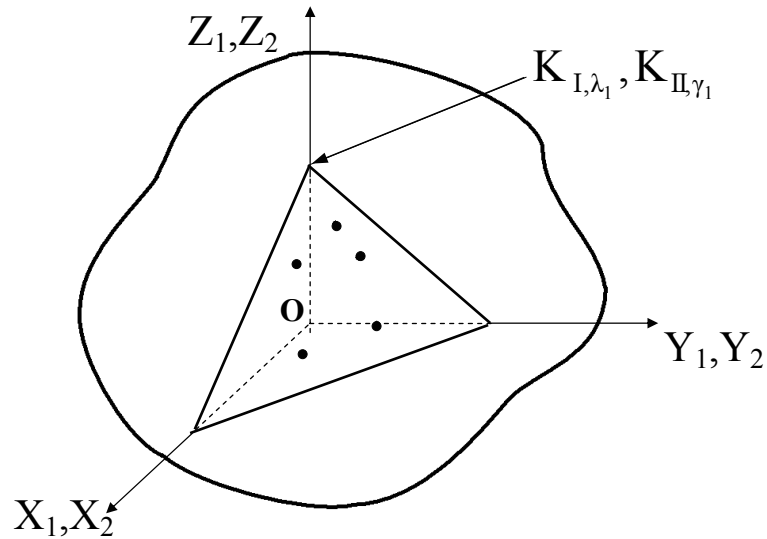


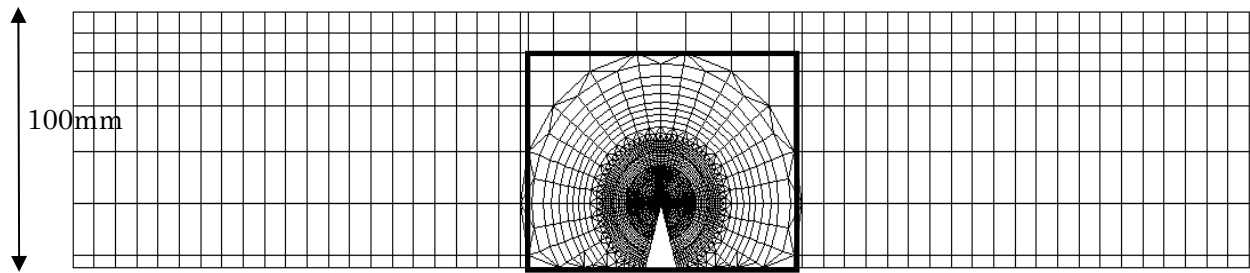
Fig.3 Least squares plane for determination of $K_{I,\lambda}$ and $K_{I,\gamma}$

Table 3 Distances from the notch tip to the strain gage positions

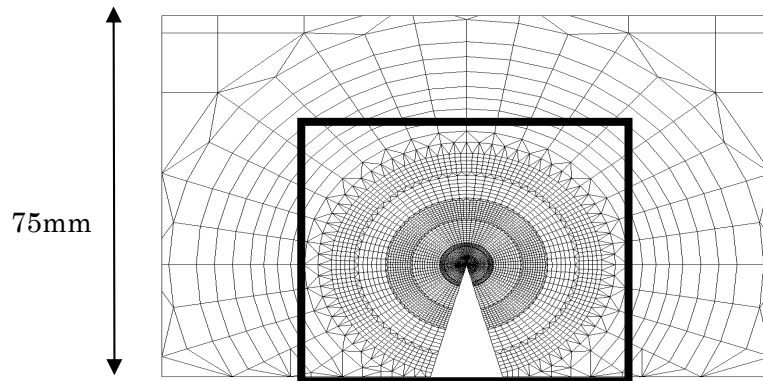
Specimen	r_{1i} (mm), $\theta_1 = 90$ deg, ($i = 1, 2, \dots, 5$)					r_{2i} (mm), $\theta_2 = -90$ deg, ($i = 1, 2, \dots, 5$)				
	r_{11}	r_{12}	r_{13}	r_{14}	r_{15}	r_{21}	r_{22}	r_{23}	r_{24}	r_{25}
A	1.78	3.78	5.78	7.78	9.78	1.65	3.65	5.65	7.65	9.65
B	1.73	3.73	5.73	7.73	9.73	1.61	3.61	5.61	7.61	9.61
C	2.24	4.24	6.24	8.24	10.24	1.87	3.87	5.87	7.87	9.87

Table 4 Strains ε_{r1i} and ε_{r2i} ($i = 1, 2, \dots, 5$) in the direction of $\theta_1 = 90$ deg and $\theta_2 = -90$ deg.

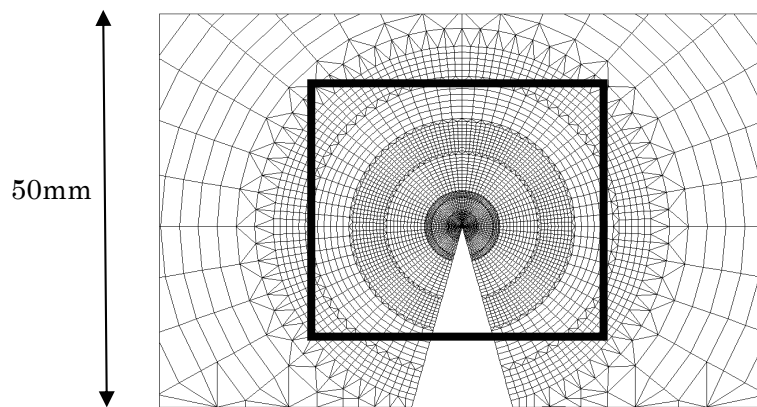
Specimen	Load (N)	$\varepsilon_{r1i} \times 10^{-6}$, $\theta_1 = 90$ deg, ($i = 1, 2, \dots, 5$)					$\varepsilon_{r2i} \times 10^{-6}$, $\theta_2 = -90$ deg, ($i = 1, 2, \dots, 5$)				
		ε_{11}	ε_{12}	ε_{13}	ε_{14}	ε_{15}	ε_{21}	ε_{22}	ε_{23}	ε_{24}	ε_{25}
A	100	71	53	43	39	36	68	49	40	36	31
	130	88	66	53	48	44	88	65	52	47	41
	160	108	81	66	58	53	105	76	63	55	49
	190	129	95	80	71	66	132	95	80	68	62
	220	154	114	95	85	78	154	113	93	81	74
B	100	74	53	43	38	33	70	52	43	42	35
	130	94	68	55	49	44	93	67	57	52	46
	160	120	86	70	63	56	118	84	72	66	57
	190	143	104	85	75	68	140	102	84	77	67
	220	161	117	95	83	74	156	116	98	89	75
C	100	65	55	47	43	40	70	54	48	41	40
	130	87	73	64	58	56	93	72	65	56	51
	160	104	88	76	69	65	114	90	81	69	63
	190	122	102	88	80	76	132	102	90	79	71
	220	147	124	106	97	89	156	122	109	95	87



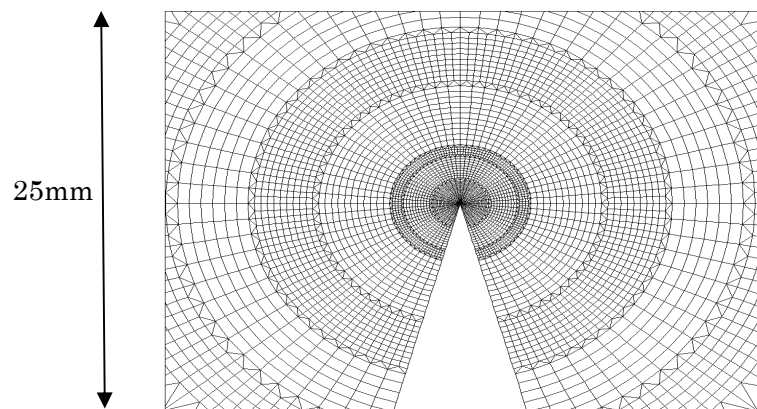
(a) A whole view of the specimen



(b) $y=75\text{mm}$



(c) $y=50\text{mm}$



(d) $y=25\text{mm}$

Fig. 4 An example of finite element mesh for $2\beta = 30\text{deg.}$ and vertical lengths of y enclosing by squares.

tip of the V-notch. Three dimensional representation of the strain fields ϵ_{rr} near the sharp V-notched plate under $P=220\text{N}$ for notch angle $2\beta = 30\text{deg}$ is shown in Fig.5. This figure shows clearly that the strain field is considerably affected by the angle θ around the V-notch. The strains from the tips of the notch to the each collocation point r_{ji} and the angle $\theta_1 = -\theta_2 = 90\text{deg}$ as shown in Fig.2 were employed in the same way as those in the case of the experiment.

5. RESULTS AND DISCUSSION

For the specimens with the three types of notch angle, the measured strains ϵ_{rji} ($j=1,2;i=1,2,\dots,5$) by strain gages in the two directions of $\theta_1 = -\theta_2 = 90\text{deg}$ are shown in Table 4. The strains

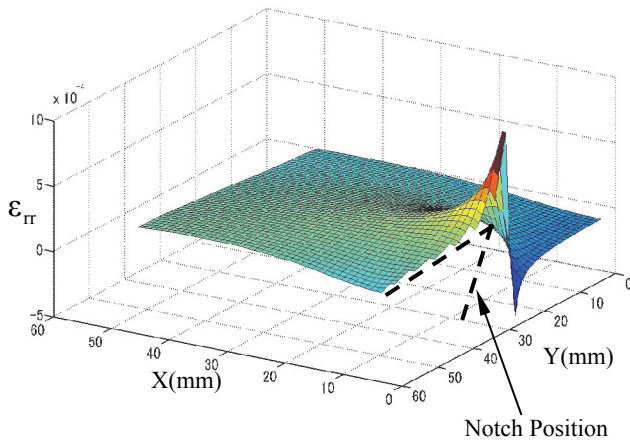


Fig.5 Three dimensional representation of the strain field near the V-notch

obtained by experiments are introduced into eqs.(36) and (37), and experimental values of K_{I,λ_1} are determined by the procedure stated above. These experimental values are compared with the finite element results.

Figure 6 shows the relation between the non-dimensional stress intensity factor K_{I,λ_1}^* and the bending stresses for the fixed values of $2\beta = 0\text{deg}$. In Fig.6, the closed form solution for an infinite plate obtained by Sih²³⁾ et.al is also indicated for the comparison with experimental and the FEA results. In this case, the effects of stress free surface of the edge and Poisson's ratio of semi-infinite plate are almost negligible²⁴⁾. It should be noted again that the K_{I,λ_1}^* is independent of the given bending stresses for the non-dimensional quantity. The results of the three cases in Fig.6 show good agreement between them, particularly the FEA result agrees well with the closed form

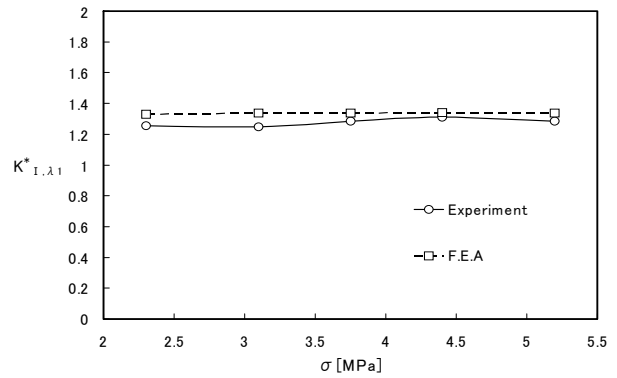


Fig.7 Comparison of the experimental and FEA results of K_{I,λ_1}^* for various bending stresses in the case of $2\beta = 30\text{deg}$.

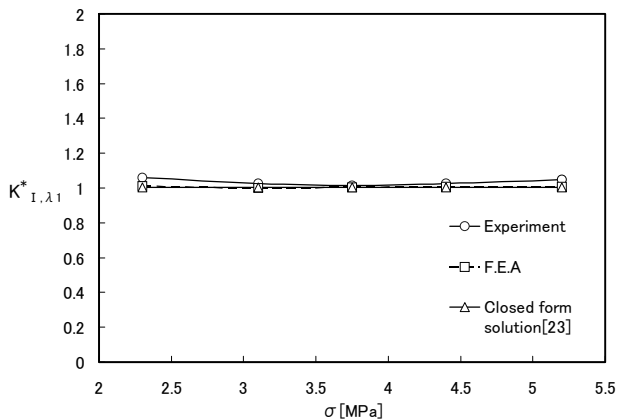


Fig.6 Comparison of the experimental and FEA results of K_{I,λ_1}^* for various bending stresses in the case of $2\beta = 0\text{deg}$.

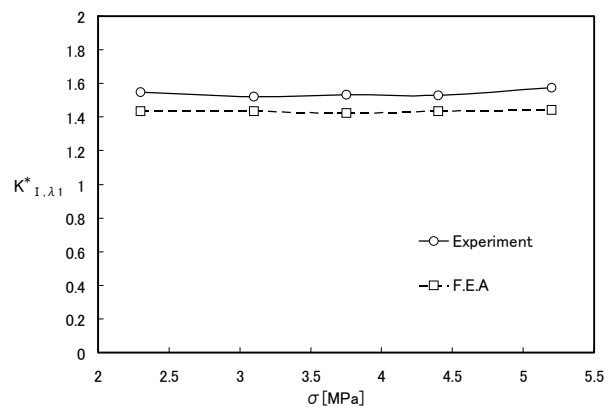


Fig.8 Comparison of the experimental and FEA results of K_{I,λ_1}^* for various bending stresses in the case of $2\beta = 60\text{deg}$.

solution. Therefore, the FEA result may be available for an indicator of accuracy of experimental results. For $2\beta = 30$ deg, a comparison of the experimental and FEA results of K_{I,λ_1}^* is shown in Fig.7. The maximum value of difference between the experimental and FEA is within 10percent. Figure 8 shows the case of $2\beta = 60$ deg. It can be seen from the figure that the maximum difference between the experimental and FEA results is larger than that of Fig.7.

6. CONCLUSION

The method of determination of the generalized stress intensity factors was developed to the bending problem on the basis of the Kirchhoff plate theory. By measuring the strains on the two lines extending from the bisector of the notch angle, we can separate the mixed mode condition into the independent generalized stress intensity factors. Experiments on the specimens with three types of notch angles $2\beta = 0$ deg, 30 deg and 60 deg for the mode I loading conditions, were performed by using strain gages, and are compared with the finite element analysis. The both results show good agreement between them.

REFERENCES

- 1) N.-A.Noda,D.-H.Chen,Y.Takase and T. Morodomi: *Evaluation of static strength by the application of mixed-mode stress intensity of angular corner*, Trans.Jap.Soc. Mech.Eng. A, Vol.64, pp.958-963,1998.
- 2) M.L.Dunn,W.Swito and S.Cunnigham: *Fracture initiation at sharp notches*,International Journal of Solids and structures,Vol.34,pp.3873-3883,1997.
- 3) F.J.Gomez and M.Elics:*A fracture criterion for sharp V-notched samples*,International Journal of Fature, Vol123,pp.163-175,2003.
- 4) P.Lazzarin and P.Livieri:*Notch stress intensity factors and fatigue strength of aluminum and steel welded joints*,Vol.23,pp.225-232,2001.
- 5) M.L.Williams:*Stress singularities resulting from various boundary conditions in angular corners of plates in extension*,Journal of Applied Mechanics, Vol.19,pp.526-528,1952.
- 6) G.Gross and A.Mendelson:*Plane elastostatic analysis of V-notched plates*,International Journal of Fature,Vol.8, pp.267-276,1972.
- 7) W.C.Carpenter: *A collocation procedure for determining fracture mechanics parameters at a corner*, International Journal of Fracture,Vol.24, pp.225-266, 1984.
- 8) K.Y.Lin and P.Tong: *Singular finite elements for the fracture analysis of V-notched plate*, Inter -national journal for Numerical Methods in Engineering, Vol.15,pp.1343-1354,1980.
- 9) M.Treifi,S.O.Oyadiji and D.K.L.Tsang: *Computations of mode I and II stress intensity factors of sharp notched plates under in-plane shear and bending by the fractal-like finite element method*, International Journal of Solids and Structures, Vol.45, pp.6468-6484,2008.
- 10) A.Portela,M.H.Aliabadi and D.P.Rooke:*Efficient boundary element analysis of sharp notched plates*: International Journal for Nemerical Methods in Engineering,Vol.32,pp.445-470,1991.
- 11) D.-H.Chen:*Stress intensity factors for V-notched strip under tension or in-plane bending*,International Journal of Fracture,Vol.70,pp.81-97,1995.
- 12) N.-A.Noda and Y.Takase:*Generalized stress intensity factors of V-shaped notch in a round bar under torsion, tension,and bending*, Engineering Fracture Mechanics, Vol.70,pp. 1447-1456,2003.
- 13) J.N.Prassianakis and P.S.Theocaris: *Stress intensity factors of V-notched elastic,symmetrically loaded, plate by method of caustics*,Journal of Physics D:Applied Physics,Vol.13, pp.1043-1053, 1980.
- 14) M.Shozu,T.Sasaki and Y.Hirose: *Effect of stress singularity by open notch on caustics method*, Journal of Japan Society for Nondestructive Inspection,Vol.44, pp.337-342, 1995.
- 15) M.Mahinfalah and L.Zakery: *Photoelastic determination of mixed mode stress intensity factors for sharp reentrant corners*, Engineering Fracture Mechanics, Vol.52,pp.639-645,1995.
- 16) X.F.Yao,H.Y.Yeh and W.Xu:*Fracture investigation at V-notch tip using coherent gradient sensing*, International Journal of Solids and Structures,Vol.43,pp. 1189-1200,2006.
- 17) T.Kondo,M.Kobayashi and H.Sekine:*Strain gage method for determining stress intensities of sharp notched strips*, Experimental Mechanics, Vol.41. pp.1-7, 2001.
- 18) T.Kondo,M.Kobayashi,K.Ishizuki and M. Sugisawa: *Determination of generalized stress intensity factors of V-notched plates under in-plane bending by using strain gages*,Transactions of Japan Society for Mechanical Engineering,A, Vol.71, pp. 1140-1146, 2005.
- 19) S.P.Timoshenko and S.Woinowsky-Krieger, *Theory of Plates and Shells*,McGrow-Hill,New York,1959.
- 20) G.N.Savin:*Stress Concentration around holes*, Pergamon Press,1961.
- 21) M.L.Williams:*The bending stress distribution at the base of a stationary crack*,Transactions of the ASME, Journal of Applied Mechanics,Vol.28, pp.78-82, 1961.
- 22) J.W.Dally and R.J.Sanford:*Strain gage method for measuring the opening-mode stress-intensity factor*,K_I, Experimental Mechanics,Vol.27,pp.381- 388,1987.
- 23) G.C.Sih,P.C.Paris and F.Erdogan:*Crack tip, stress-intensity factors for plane extension and plate bending problems*,Transactions of the ASME, Journal of Applied Mechanics,Vol.29, pp.306-312. 1962.
- 24) R.Roberts and T.Rich: *Stress intensity factors for*

plate bending, Transactions of the ASME, Journal of Applied Mechanics, Vol.34, pp.777-780. 1967.

Appendix

$$Z_1(\varepsilon_{rji}, r_{ji}) = \sqrt{2\pi} \left[\frac{\varepsilon_{r1i} \cdot r_{1i}^{1-\gamma_1} + \varepsilon_{r2i} \cdot r_{2i}^{1-\gamma_1}}{f_{r1}(\lambda_1, \alpha, \theta_1) \cdot (r_{1i}^{\lambda_1-\gamma_1} + r_{2i}^{\lambda_1-\gamma_1})} \right]$$

$$Z_2(\varepsilon_{rji}, r_{ji}) = \sqrt{2\pi} \left[\frac{\varepsilon_{r1i} \cdot r_{1i}^{1-\lambda_1} - \varepsilon_{r2i} \cdot r_{2i}^{1-\lambda_1}}{f_{r2}(\gamma_1, \alpha, \theta_2) \cdot (r_{1i}^{\gamma_1-\lambda_1} + r_{2i}^{\gamma_1-\lambda_1})} \right]$$

(a),(b)

$$A_1 = \sqrt{2\pi} \frac{f_{r3}(\omega, \theta_1)}{f_{r1}(\lambda_1, \alpha, \theta_1)}, A_2 = \sqrt{2\pi} \frac{f_{r3}(\omega, \theta_1)}{f_{r2}(\lambda_1, \alpha, \theta_2)}$$

(c),(d)

$$B_1 = \sqrt{2\pi} \frac{f_{r3}(\omega, \theta_2)}{f_{r1}(\lambda_1, \alpha, \theta_1)}, B_2 = \sqrt{2\pi} \frac{f_{r3}(\omega, \theta_2)}{f_{r2}(\lambda_1, \alpha, \theta_2)}$$

(e),(f)

$$X_1 = \frac{r_1^{1-\gamma_1}}{r_1^{\lambda_1-\gamma_1} + r_2^{\lambda_1-\gamma_1}}, X_2 = \frac{r_1^{1-\lambda_1}}{r_1^{\gamma_1-\lambda_1} + r_2^{\gamma_1-\lambda_1}}$$

(g),(h)

$$Y_1 = \frac{r_2^{1-\gamma_1}}{r_1^{\lambda_1-\gamma_1} + r_2^{\lambda_1-\gamma_1}}, Y_2 = \frac{r_2^{1-\lambda_1}}{r_1^{\gamma_1-\lambda_1} + r_2^{\gamma_1-\lambda_1}}$$

(i),(j)

(Received October 1, 2009)